Comparative cytotoxicity of kaolinite, halloysite, multiwalled carbon nanotubes and graphene oxide

Elvira Rozhina,[1] Svetlana Batasheva,[1] Regina Miftakhova,[1] Xuehai Yan,[2] Anna Vikulina,[3] Dmitry Volodkin,[4] Rawil Fakhrullin[1*]

[1]*Institute of Fundamental Medicine and Biology, Kazan Federal University, Kreml uramı 18, Kazan, Republic of Tatarstan, RF, 420008*

[2]*State Key Laboratory of Biochemical Engineering, Institute of Process Engineering, Chinese Academy of Sciences, Beijing 100190, P. R. China*

[3]*Fraunhofer Institute for Cell Therapy and Immunology, Branch Bioanalytics and Bioprocesses, Am Muhlenberg 13, 14476 Potsdam-Golm, Germany.*

[4]*School of Science and Technology, Department of Chemistry and Forensics, Nottingham Trent University, Clifton Lane, Nottingham NG11 8NS, UK.*

Corresponding author's email: kazanbio@gmail.com

Abstract

This study aimed at comparative examining of the interactions between conventionally used clay and carbon nanomaterials and human lung adenocarcinoma cells (A549 cells). The following platy and tubular nanomaterials were tested: carbon nanoparticles, i.e. multi-walled carbon nanotubes (MWCNTs) and graphene oxide nanosheets (GO) as well as nanoclays, i.e. halloysite nanotubes (HNTs) and kaolinite nanosheets (Kaol). Nanoparticle physicochemical properties and their internalisation into cells were examined using dynamic light scattering as well as atomic force, 3D laser scanning confocal and darkfield hyperspectral microscopies. Biological aspects of the nanomaterial-cell interaction included assessment of cellular toxicity, DNA damage,

metabolic activity, and physical parameters of the cells. Regardless of a shape, carbon nanomaterials demonstrated cell surface adsorption, but negligible penetration into cells compared to nanoclays. However, carbon nanomaterials were found to be the most toxic for cells as probed by the MTS assay. They also turned out to be the most genotoxic for cells compared to nanoclays as revealed by the DNA-Comet assay. GO significantly increased the fraction of apoptotic cells and was the most cytotoxic and genotoxic nanomaterial. Comparison of flow cytometry and MTS data indicated that a cytotoxic effect of MWCNTs was not associated with increased cell death, but was rather due to a decrease in cell metabolic activity and/or proliferation. Finally, no significant effect of the shape of the tested nanomaterials on their internalization and cytotoxicity was revealed.

Key words: halloysite, kaolinite, multiwalled carbon nanotubes, graphene oxide, cytotoxicity, genotoxicity

1. Introduction

The scope of nanoparticle (NP) applications and the types of nanomaterials used are constantly expanding. A particular attention is drawn to the nanospheres and nanotubes as potent systems for drug delivery (Lazzara et al., 2017). Nanotechnology has had an extremely important impact on nanobiomedicine, as well as on the diagnostics and treatment of various diseases (Marcano et al., 2018). The advantage of nanoparticles as carriers is their ability to bind certain ligands and deliver them to a specific cell population (Balthasar et al., 2005). They can also facilitate the penetration of drugs through the cellular membrane (Amai and Tsuji, 2000). Multifunctional carriers represented by carbon nanoparticles (Mohajeri et al., 2018; Choi et al., 2018), silicon- (Rahikkala et al., 2018) and chitosan- (Li et al., 2018) based nanomaterials, lipid and polymer-based nanoparticles (Allen and Cullis 2004) were described. The use of nanomaterials in the

treatment of cancer is promising since they can release drugs at required conditions: a given pH, temperature change, light or ultrasound (Thambi and Park, 2014). Nanostructures are also used for diagnostics of diseases and as tools for monitoring the tissue repair (LaVan et al., 2003).

The appearance and wide distribution of nanomaterials of various forms, chemical composition, and charge invoked the emergence of a new science - nanotoxicology - which aims at understanding the physicochemical properties of nanomaterials and assessing their toxic effects on humans and the environment (Xia et al., 2006). Clinical and experimental studies show that the properties of some nanomaterials, along with their value for materials science, can have a negative effect on human tissues and therefore their toxicological effects require a close attention. The effect of the nanomaterial shape on toxicity is still not fully understood, although numerous studies suggest that there exists a relationship between the substrate shape and its toxicity (Oh et al., 2010, Sharifi et al., 2012; Gatoo et al., 2014; Jeevanandam et al., 2018).

In this study we compare the toxic potential of nanoparticles having tubular and platy morphologies. They include carbon-based nanoparticles, i.e. multi-walled carbon nanotubes (MWCNTs) and graphene oxide (GO) nanosheets as well as clays, i.e. halloysite nanotubes (HNTs) and planar kaolinite particles (Kaol). Graphene is an allotrope of carbon consisting of a single layer of carbon atoms arranged in hexagonal lattice (Geim and Novoselov, 2007). One of the most important graphene derivatives is GO (Park and Ruoff, 2009), which has a large number of oxygen atoms on its surface in the form of carboxyl groups, epoxy groups, and hydroxyl groups (Dreyer et al., 2010). GO is a highly appraised material in electronics, energy, and materials science (Stankovich et al., 2006). Recently GO has actively been considered as an agent for biomedical research and drug delivery (Liu et al., 2008; Su et al., 2013; Chen et al., 2012). Single or multiple graphene sheets rolled into cylinders form single-walled and multi-walled CNTs,

77 respectively. CNTs are widely known for their unique physicochemical properties and
78 practical applications (Yang et al., 2012); GO also play an important role in drug delivery
79 as a carrier system (Kayat et al., 2011). Since the multi-ton production and use of these
80 nanoparticles is envisioned, it is important to better understand and probe a possible
81 toxicity of CNTs.

82 Kaolinite minerals are among the most common clay minerals on Earth. They are 1:1
83 phyllosilicates of variable morphology with the theoretical formula of $Al_2Si_2O_5(OH)_4$ x
84 nH_2O, where n = 0 and 2, for kaolinite and hydrated halloysite, respectively. The minerals
85 find wide practical application for the transfer of drugs and enzymes, in cosmetics and
86 tissue engineering, and are used as a suspending agent, white pigment and an additive
87 to various materials to improve their mechanical strength, electrical resistance and
88 appearance (Awad et al., 2017). Kaolinite is generally represented by stacked platelets
89 which are hydrophilic and easily dispersible in water. Ionic and/or polar nonionic
90 surfactants can be applied to the surface of kaolinite to make it hydrophobic or
91 organophilic (Murray, 2000). Halloysite is found in soils and rocks and is a multilayer
92 nanotube with an internal cavity diameter of about 50 nm and a length of up to 1 μm.
93 HNTs were also proposed as drug, cosmetics and gene delivery agents (Lvov et al., 2016;
94 Panchal et al., 2018; Micó-Vicent et al., 2018; Massaro et al., 2019; Batasheva et al.,
95 2020), as well as components of cell capturing devices (Kryuchkova et al., 2020) and
96 tissue engineering scaffolds (Naumenko and Fakhrullin, 2019).

97 Not surprisingly, carbon and clay nanotubes and nanoplates are currently a kind of
98 competing nanomaterials in the field of biomedicine. Although the unique properties of a
99 given nanomaterial mostly determine the scope of its application, all the benefits
100 conferred by the nanomaterial use must be weighed against its toxic potential. Numerous
101 studies have already been published on the toxicity of pristine and surface-modified
102 carbon and clay nanomaterials (Magrez et al., 2006; Cornejo-Garrido et al., 2012; Yang

et al., 2013; Cervini-Silva et al., 2013, 2015, 2016; Maisanaba et al., 2015; Kryuchkova et al., 2016; Tarasova et al., 2019; Rozhina et al., 2020). However, the toxicity results obtained in different studies are sometimes contradictory and difficult to collate and compare because of variability in cell lines used, cell culture and other conditions. Systematic investigation is needed in which carbon and clay nanomaterials would be compared in one study using the same cell type and at the same conditions.

Recently a comparison of toxicity of MWCNTs and HNTs to human umbilical vein endothelial cells (HUVECs) *in vitro* and blood vessels of mice *in vivo* was reported (Wu et al., 2020). All of the toxic effects were more pronounced for MWCNTs in comparison with HNTs, implying that HNTs are probably safer nanocarriers compared with MWCNTs (Wu et al., 2020). However, the observed nanoparticle effects can be cell-type dependent (Pacurari et al., 2008) and greater safety of HNTs in comparison with MWCNTs should be verified in other cell types. In this study, for the first time the effects of carbon and clay nanomaterials of different shapes on human lung carcinoma cell line (A549) were compared side by side. The model of lung cells was chosen because inhalation is not only the most likely route of environmental nanoparticles exposure but the lung can be exposed to nanoparticles that are introduced to the body by any other administration route including gastrointestinal absorption and direct injection (Card et al., 2008). Cancer cell lines are widely used in the nanomaterial toxicity screenings because of their unlimited replication ability and wide distribution among researchers around the world, while their cell-to-cell variability can be addressed by application of statistical analyses.

2. Materials and methods

2.1. Materials

Kaol nanoparticles, MWCNTs and GO aqueous solutions, propidium iodide (PI) were purchased from Sigma Aldrich. All reagents were of analytical grade, and were used as

received without further purification. HNTs were received from Applied Minerals INC (NY, USA).

2.2. Particle characterization

NPs were resuspended in ultrapure H_2O at a concentration of 40 mg mL^{-1}. A sonication in a US-bath (Sonics & Material Inc., New Town, CT, USA) at 30 W for 10 min was applied to avoid NP aggregation. Hydrodynamic diameter and zeta-potential were determined at 25°C in water using dynamic light scattering (DLS) in a Zetasizer Nano-ZS, Model ZEN3600 equipped with 633 nm laser of power of 4.0 mW (Malvern instruments Ltd., Malvern, UK).

2.3. Cell culture

A549 cells were obtained from American Type Culture Collection (ATCC, Rockville, Maryland, USA) and cultured in minimal Eagle's medium Alfa (aMEM) (Paneco, RF) culture medium supplemented with 10% (v/v) fetal bovine serum (Gibco) and 100 UmL^{-1} penicillin and 100 µg mL^{-1} streptomycin at 37°C in a humidified atmosphere containing 5% CO_2 and 95% air.

2.4. Microscopic observations of NPs and cells

Dark field microscopy images were obtained using a CytoViva® enhanced dark-field condenser attached to an Olympus BX51 (Japan) upright microscope equipped with fluorite 100× objectives and a DAGE CCD camera. Extra-clean dust-free Nexterion® glass slides and coverslips (Schott, Mainz, Germany) were used for enhanced dark-field microscopy imaging to minimize dust interference. For hyperspectral imaging of NPs and cell samples illuminated in the dark-field mode, scanning of the sample was performed automatically using a ProScan III (Prior) scanning module attached to the specimen table. Full field of view (901 image lines) images were collected at 0.1 s exposure time at

maximal halogen bulb light intensity. The hyperspectral data were collected using a Specim V10E spectrometer and PCOPixelFly CCD video camera. Spectra were collected within the 400 – 1000 nm region, spectral resolution was 2 nm. Hyperspectral data collection and mapping was performed using ENVI 4.8 software (Harris & Geospatial Solutions). Spectral libraries were obtained for pure nanoparticles (n = 20), which were then matched with hyperspectral images obtained from cells with internalized nanoparticles. This was done using the internal spectral mapping algorithm to determine the spectral matches between the image pixels in hyperspectral image of the cells and previously obtained nanoparticles spectral libraries. Spectral angle mapper threshold of 0.3 radians was used. Individual colors were assigned to the pixels spectrally matching the NPs spectral signatures. ImageJ freeware (NIH) was used to calculate the area percentage of each individual color (expressed as number of pixels and percent of the whole image area).

The atomic force microscopy (AFM) images were obtained with Dimension Icon microscope (Bruker, USA) operating in the PeakForce Tapping mode. The ScanAsyst-air (Bruker) probes (nominal length 115 µm, radius of tip 2 nm, spring constant 0.4 N m^{-1}). The images were obtained with 512-1024 lines/scanning at a speed of 0.8-0.9 Hz to provide high resolution images and display mechanical properties. Images were collected in the height (topography), peak force error, Young's modulus and adhesion imaging channels. The received data was processed using Nanoscope Analysis v.1.7. software (Bruker).

The topography of cells was studied using a laser scanning confocal microscope (LSCM) Keyence VK-X150 (Keyence, USA), as reported elsewhere (Panchal et al., 2018). The data obtained were processed using VK-Analyzer software (Keyence, USA).

2.5. Cell viability

The cell viability was evaluated by CellTiter 96® AQueous One Solution Cell Proliferation Assay, MTS (ProMega) according to the standard protocol. Briefly, A549 cells were seeded in the 96-well plates (2×10^3 cells per well) and incubated for 24 h. Then, NPs were added to the cells at different concentrations (11, 33, 100, 300 and 900 μg mL^{-1}). After 24 h of incubation cells were subjected to the incubation with MTS reagent and optical density (OD) of each well at 490 nm and 540 nm was measured by a Tecan Infinite 200Pro (Tecan Trading AG). The cell viability (% to control) is expressed as the percentage of (ODtest − ODblank)/(ODcontrol − ODblank), where ODtest is the optical density of the cells exposed to a nanoparticles sample, ODcontrol is the optical density of the control sample and ODblank is the optical density of the wells without A549 cells.

2.6. Apoptosis assay

Apoptosis kit (FITC Annexin V Apoptosis Detection Kit I, Invitrogen) was employed to detect apoptotic and necrotic cells. A549 cells were seeded in 6-well plates (1×10^5 cells per well) and incubated for 24 h. The NPs samples were added to the cells at the concentration of 100 μg mL^{-1} and incubated for another 24 h. A549 cells were collected, washed twice with PBS, and re-suspended in Annexin V buffer (1×10^6 cells mL^{-1}) and stained with 5 μL of FITC-conjugated Annexin V (Annexin V-FITC) and 5 μL of propidium iodide. Cells were analyzed on FACS Aria III flow cytometer (BD Biosciences, USA).

2.7. Comet (single-cell gel electrophoresis) assay to detect damaged DNA

The Comet assay was performed according to protocol described (Nandhakumar et al., 2011). Briefly, a stock lysis solution was prepared: 10 мM Tris, 2.5 M NaCl, 100 мM EDTA, pH 10. Working lysis solution was cooled down to 4°C before use. The solution of low-melting agarose was prepared (0.5 %). Cell suspension (about 10^5 cells) was mixed with low-melting agarose at 37°C and put on slides. Then the cells were distributed on the glass with the tip and left at 4°C for 10 minutes. The cells were lysed for 45 minutes

at 4°C and washed with TAE-buffer. Then electrophoresis was carried out for 20 min at a field strength of (1 - 10) V cm^{-1} and a current strength of ~ 300 mA. The glasses were placed into 70% ethyl alcohol and washed with distilled water for 5 minutes at room temperature. The cells were stained with ethidium bromide (EtBr). The nuclear damage was analyzed with confocal microscopy LSM 780 (Carl Zeiss, Germany). For each treatment at least 100 of DNA comets were randomly analyzed. Data processing was implemented with the Comet Assay IV (Instem, UK) software.

2.8. Statistical analysis

The data is expressed as the mean ± standard deviation. The Student's t-test was applied to measure statistical differences in the data. A p-value of less than 0.05 was regarded as statistically significant.

3. Results

3.1. Physicochemical characterization of particles

The effects of flat and tubular NPs on biological cells were analysed and compared in this study for different NPs. The study of electrophoretic mobility as well as the visualisation of nanomaterials using dark field microscopy allowed determination of the stability of the NP suspensions used and their dimensional characteristics (Table 1).

Table 1. ζ-Potentials and sizes of nanoparticles measured by dynamic light scattering and AFM (Dispersions of the nanomaterials in deionized water were used for the measurements of ζ-Potentials and hydrodynamic diameters).

Nanomaterial	Zeta potential (mV)	Size	
		DLS (d.nm)	AFM (nm)
Halloysite nanotubes	-31.8±3.7	310.5±4.1	626.5±176.4
Kaolinite	-31.5±0.6	753.1±34.9	526.9±206.8
Carbon nanotubes	-26.8±0.1	254.4±10.1	414.3±79.3
Graphene oxide	-48.6±2.4	1944±89.1	1065.8±251.5

222

223 Carbon and clay nanotubes were similar in their size and zeta-potential. However, the
224 absolute value of the MWCNTs zeta-potential was lower than 30 mV, potentially
225 determining their lower colloidal stability. GO particles demonstrated the largest size and
226 the highest negative zeta-potential. It is hard to determine the real size of NPs using DLS
227 because the NPs tested here have different morphology. However, DLS did not reveal
228 any significant aggregation of NPs and the NP dimensions have further been probed
229 using AFM. The tubular morphology of halloysite and carbon nanotubes as well as platy
230 morphology of Kaol and GO particles was confirmed by AFM analysis (Figure 1).

231 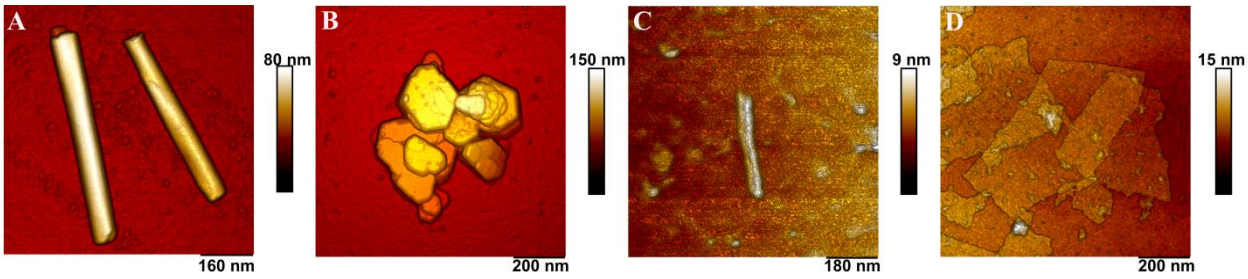

232 **Figure 1.** AFM images demonstrating the morphology nanoclays and carbon
233 nanomaterials used in this study: HNTs (A); Kaol (B); MWCNTs (C); GO (D). All NPs were
234 prepared as water suspensions and further air-dried on clean glass surfaces.

235 Dark-field microscopy observations proved that the nanotubes and nanoplates were well-
236 dispersed and did not produce any aggregates during incubation with cells (Figure 2).

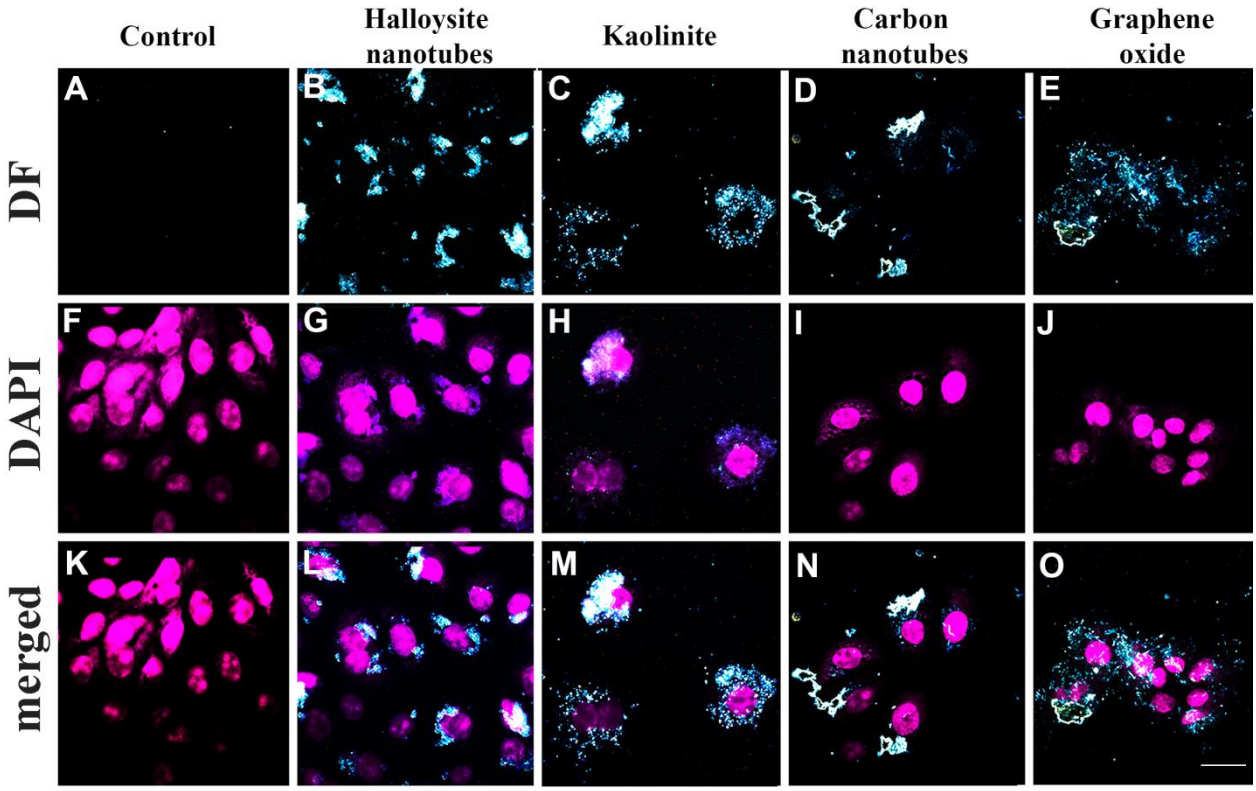

Figure 2. Dark-field (A-E), fluorescence (F-J) and merged dark-field and fluorescence microscopy (K-O) images of NPs uptake by A549 cells after 24 h incubation. Control A549 cells (A, F, K) and A549 cells incubated with HNTs (B, G, L); Kaol (C, H, M); MWCNTs (D, I, N); GO (E, J, O). The nuclei of cells were stained with DAPI (artificial color). Scale bar is 25 μm.

The dark-filed microscopy is a convenient tool for visualisation and detection of nanomaterials of different chemical nature and shape, based on registration of the scattering signals of nanoparticles (Xu et al., 2020). Here, we managed to visualise the carbon and halloysite nanotubes, kaolinite and graphene oxide in adherent A549 cells.

3.2. Cell penetration and cytotoxicity of NPs

Initially, we visualised the distribution of nanomaterials using dark-field microscopy. Then, for each type of NPs, a hyperspectral profile of reflected light was obtained in the range from 400 to 1000 nm, as described earlier (Akhatova et al., 2019) (Figure S1). The reflectance spectra can be used as a signature allowing identification of specific NPs,

such as noble metal nanoparticles (Basnet et al., 2016), CNTs (Smith et al., 2014), graphene oxide (Kryuchkova et al., 2018) and nanoclays (Khodzhaeva et al., 2017) in biomaterials.

The intensity-normalised spectra from Figure S1 were then used to identify NPs in A549 cells incubated for 24 h with NPs at concentration of 100 μg mL^{-1} and fixed with paraformaldehyde. However, it was reported that cell fixation procedure itself can alter the NP interaction with cells (Richard et al., 2003). Therefore, cell penetration by NPs was additionally studied in non-fixed cells that were only washed three times with PBS to remove culture media and non-attached NPs. Similar results on NP localization were obtained for both fixed and non-fixed cells. The use of dark-field and hyperspectral microscopies revealed poor absorption of tubular MWCNTs and planar GO by A549 cells, in contrast to aluminosilicates with different surface geometries (Figure S2). Both planar and tubular forms of nanoclays were successfully visualised in the cell interior, but both types of carbon nanomaterials, despite the high intensity of the spectra, could hardly be identified in the cells. Before the analysis, the cells were thoroughly washed with a buffer three times in order to remove freely floating and weakly adhered to the cell surface aggregates of nanoparticles and analyze only those nanomaterials that were inside the cells or strongly interacted with the cell surface (Figure 3).

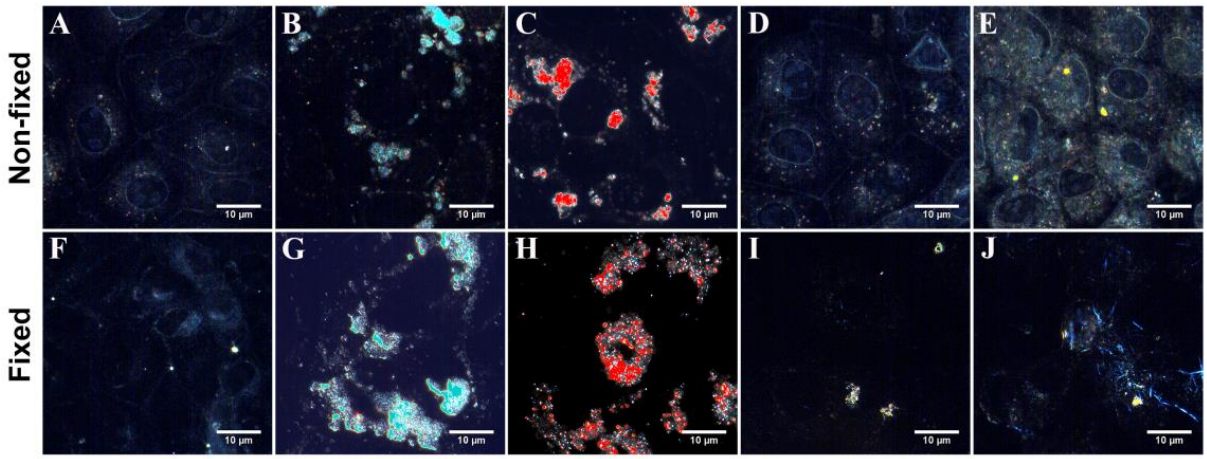

Figure 3. The mages of A549 cells obtained using dark-field and hyperspectral microscopy after 24 h of incubation with NPs: native cells (A, F); A549 cells incubated with halloysite nanotubes (B, G); kaolinite (C, H); carbon nanotubes (D, I); graphene oxide (E, J). Upper and lower rows of images correspond to non-fixed and fixed cells, respectively.

The changes in the morphology and roughness of cells after 24 h incubation with nanomaterials (at concentration of 100 μg mL^{-1}) were also investigated using AFM and 3D LSCM (Figure 4). The combination of different microscopic methods allows obtaining more information on the interaction of NPs of various shapes and nature with cell membranes. While 3D LSCM is completely non-contact and better than AFM in terms of operability, it has lower measurement resolution and thus is less powerful than AFM in detecting nanoparticles present on the cell surface. Therefore, here we have applied both AFM and 3D LSCM to get insights of cell surface morphology both at microscale and nanoscale.

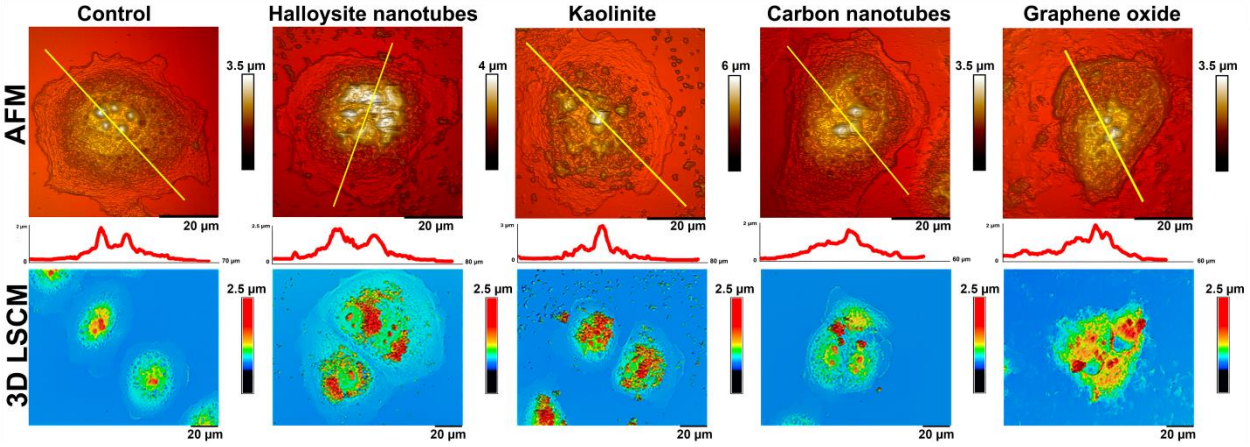

Figure 4. Morphology of intact A549 cells (A, F) and A549 cells incubated with HNTs (B, G), Kaol (C,H), MWCNTs (D, I), GO (E,J). Upper row of images shows the results obtained usinf AFM and the lower row by 3D LSCM. In between the images' rows, profiles taken along corresponding lines of the AFM images are presented.

Introduction of HNTs and Kaol into the incubation medium resulted in 2.23- and 1.86-times increase in the cell volume compared to the control experiment, respectively. After the introduction of MWCNTs and GO, a change in the cell volume of 1.68 and 1.14 times was observed, respectively. The data obtained can indicate the variable intensity of NP absorption by cells, as it was described previously for the increase in cell volume due to endocytosis of SPION (Zhou et al., 2018). Higher volume increase in the case of cell exposure to nanoclays points to their more efficient internalisation by cells; it is opposite to carbon nanomaterials which did not significantly affect the cell volume. However, the presence of carbon nanomaterials increased the cell surface roughness (R_a – average roughness) assessed using 3D-microscopy. The following R_a were obtained: A549 control cells (R_a=0.014±0.005 µm), A549-MWCNTs (R_a=0.039±0.02 µm), A549-GO (R_a=0.029±0.006 µm). No statistically significant differences in cell surface roughness were observed between control cells and cells incubated with nanoclays: A549-HNTs (R_a=0.018±0.005 µm), A549-Kaol (R_a=0.035±0.010 µm), when calculated using the Student's t-test at the significance threshold $P < 0.05$.

To assess the cytotoxic potential of the studied nanomaterials, we evaluated the relationship between the applied dose of NPs and the viability of cells after 24 h incubation with nanomaterials. This was done using the MTS test with 3-(4,5-dimethylthiazol-2-yl)-5-(3-carboxymethoxy-phenyl)-2-(4-sulfophenyl)-2H-etrazolium inner salt (Figure 5).

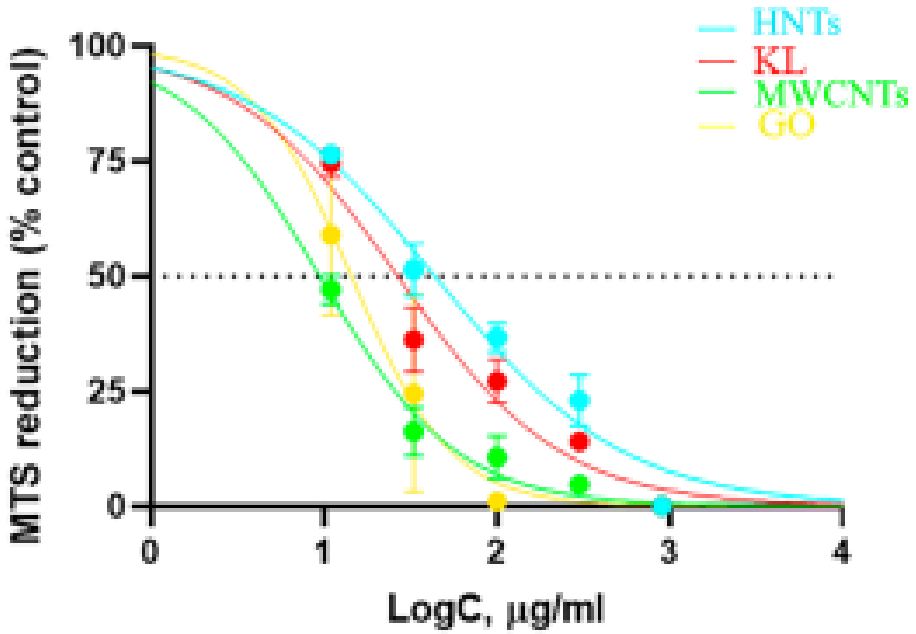

Figure 5. The reduction of MTS by A549 cells after 24 h incubation with NPs. All NPs show a decrease in MTS reduction by cells in a dose-dependent manner with semi-inhibitory concentrations indicated by a dotted line. Error bars represent the standard deviation of three parallel and independent tests.

The dose-dependent inhibiting effect of all the studied types of nanomaterials was revealed and IC50 for each nanomaterial type was determined. MWCNTs and GO were found to be the most toxic nanomaterials for cells. A semi-inhibitory concentration of 9.4±0.9 µg ml^{-1} for MWCNTs and 14.4 ±0.9 µg ml^{-1} for GO was found, compared to 43.69±2.30 µg mL^{-1} for HNTs and 26.6±1.1 µg mL^{-1} for Kaol, which indicates a lower toxicity of aluminosilicates for A549 cells, in comparison with carbon materials. Additionally, MWCNTs were more toxic than GO plates according to the results of MTS test.

However, the rate of tetrazolium reduction depends on viable cell number (which is determined by both cell death and cell proliferation level) and general metabolic activity of cells (Berridge and Tan, 1993; Berridge et al., 2005). Thus, cell viability data obtained

by MTS assay must be corroborated by a more direct viability probing method such as flow cytometry. Additionally, using flow cytometry and cell staining with annexin and propidium iodide, the mechanism of the toxic effect of the studied nanomaterials can be evaluated (Figure 6).

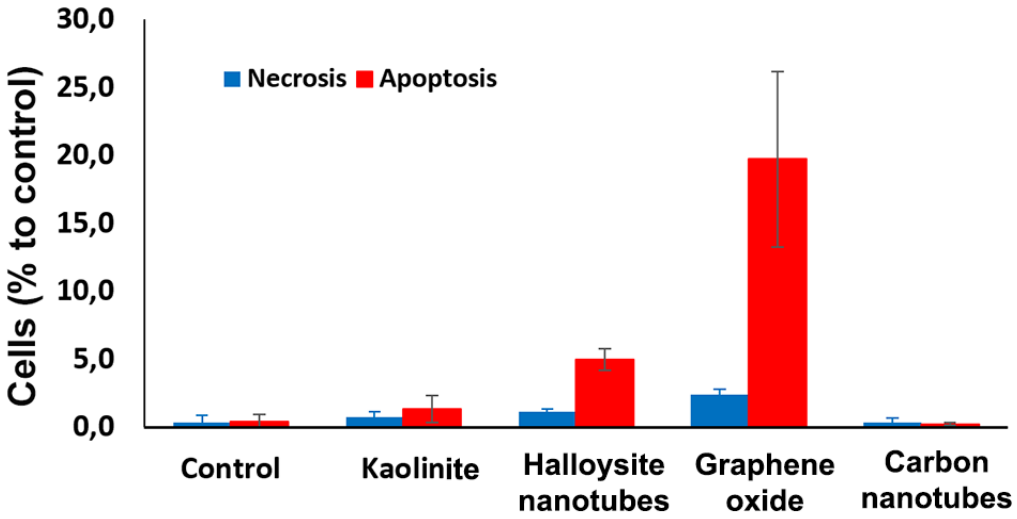

Figure 6. Effect of carbon and clay nanomaterials on cell viability assessed by flow cytometry. The fraction of apoptotic and necrotic cells is presented as a percentage to a total cell number.

According to the flow cytometry data, MWCNTs did not induce cell death and apoptosis at the concentration of 100 μg mL^{-1}. However, the cell death is not the only indicator of cellular dysfunction and thus nanomaterial toxicity to cells. MWCNTs significantly inhibited the reduction of tetrazolium by cells in MTS assay, which implies the negative impact of carbon nanotubes on the cell proliferation or metabolic activity. As the rate of tetrazolium reduction depends on viable cell number and general metabolic activity, it can be concluded that a high cytotoxic effect of MWCNT demonstrated in the MTS assay was not associated with cell death, but was rather due to a decrease in cell metabolic activity or proliferation.

Another reason of the discrepancy between the results of cell viability assessment by a colourimetric test and flow cytometry can be related with CNT interaction with indicator dyes. A fake strong cytotoxic effect of CNT within the MTT assay was observed previously in CNT treated A549 cells (Wörle-Knirsch et al., 2006), which was related to a reduction in MTT-formazan content in solution because of formation of insoluble MTT-formazan crystals covering the nanotubes. The authors did not find a similar effect when using water-soluble MTT analogues (like WST-1) and recommended water-soluble dyes for cell viability testing in the presence of carbon nanotubes (Wörle-Knirsch et al., 2006). MTS, used in our study, is another water-soluble analogue of MTT, which was previously applied for assessment of CNT cytotoxicity (Guo et al., 2008; Meindl et al., 2013). However, even water soluble MTT analogues (WST-1) can interact with CNTs, which may result in false positive toxic effect similar to that observed in the MTT assay (Casey et al., 2007). Moreover, the authors concluded that a whole range of indicator dyes (Coumassie Blue, Alamar Blue TM, Neutral Red, MTT and WST-1) were not appropriate for the quantitative toxicity assessment of carbon nanotubes because of nanotubes interaction with the dyes, resulting in the reduction of the associated absorption/fluorescent emission (Casey et al., 2007). Thus, using only colourimetric assays is obviously not enough for evaluating the cytotoxicity of carbon nanotubes.

In case of GO, high cytotoxicity observed in MTS test was confirmed by flow cytometry data. The highest proportion of dead (primarily apoptotic) cells was detected after the addition of graphene oxide, which coincides with the earlier data (Rozhina et al., 2019). The tubular nanoclay induced a higher rate of cell death compared to the platy one, according to the flow cytometry data, but the inhibition of tetrazolium reduction was higher in case of kaolinite, evidencing lower proliferation and/or cell metabolic activity in the presence of platy nanoclays.

3.3. Genotoxicity of carbon and clay nanoparticles

Next, the genotoxicity of nanomaterials was investigated using the DNA-Comet assay (Figure 7). Comet assay (single cell gel electrophoresis assay) is a sensitive and effective method for analyzing DNA damage in cells (Dhawan et al., 2009) and it is the most used assay in assessing the genotoxic potential of nanomaterials (Azqueta and Dusinska, 2015). In this method DNA damage becomes visible as a "tail" of DNA fragments migrating in an electric field away from the undamaged DNA remaining within the nucleoid. Analysis of the intensity of the comet tail relative to the nucleoid is related to the number of DNA breaks that have occurred in a particular cell. By counting the relative intensity of tail and nucleoid in 100 cells per sample, we evaluated the percentage of DNA damage in each sample. The percentage of DNA damage was presented as a diagram, where 100 is a maximal DNA content in "tail" and 0 is an absence of DNA damage (Figure 7, C). As a positive control the doxorubicin (2 mg mL^{-1}) was used, which induces specific oxidative damage of DNA.

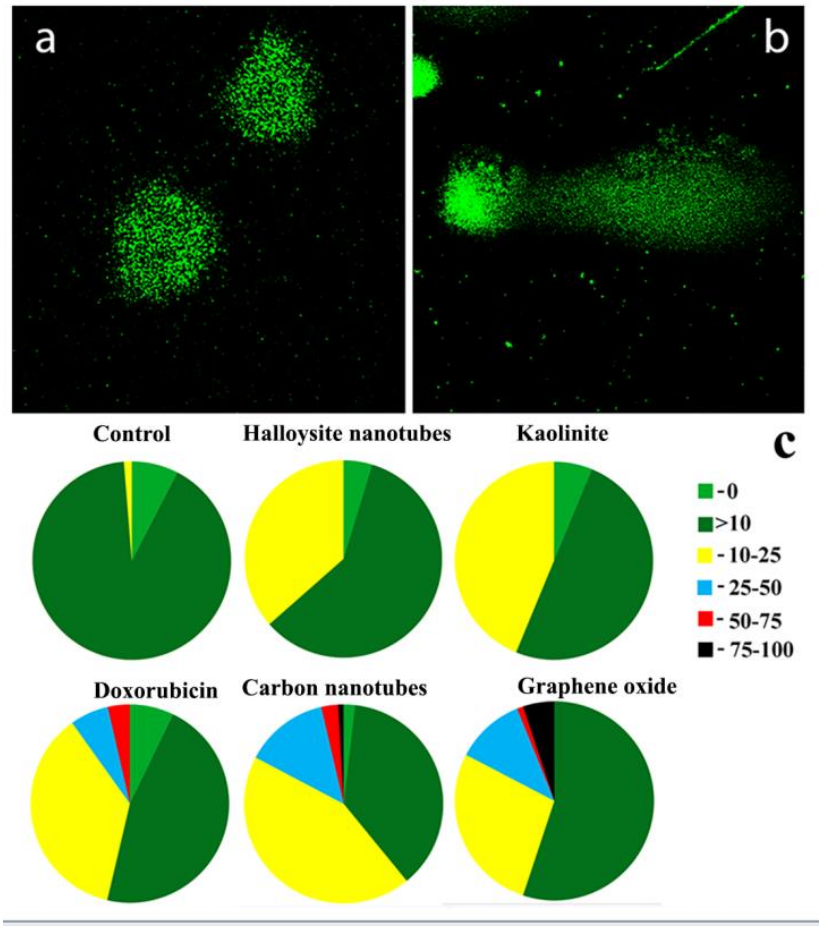

Figure 7. DNA damage in cells after 24 h incubation with carbon and clay nanomaterials assessed by the Comet assay. Images of typical "comets" representing intact DNA (a) and damaged DNA (b). Circular charts (c) displaying fractions of cells with various degrees of DNA damage (100 - maximal DNA content in the comet tail, 0 – no tail). Doxorubicin was used as a positive control.

The minimal cell DNA damage was observed after introduction of kaolinite and halloysite (100 μg mL^{-1}) into the cultivation medium. The introduction of GO and MWCNTs led to an increase in the degree of DNA degradation, while in control, DNA damage was less than 10%. As can be seen in the graph, the addition of GO to the medium led to an almost complete degradation of DNA in some cells. Thus, both forms of natural nanoclay (planar and tubular) turned out to be the least genotoxic for cells.

4. Discussion

The morphology of NPs, their size and chemical nature are known to play important roles in the delivery of therapeutic agents (Wang et al., 2018). Despite the widespread use of nanoscale materials in various fields, there are numerous reports of their side effects on biological systems and cell compartments. According to results obtained in this study, both platy and tubular carbon nanomaterials possess higher general toxicity than nanoclays for A549 cells. To date, there is a lot of inconsistency in the published results on MWCNTs toxicity studies due to permutations in NP dimensions, composition and surface chemistry, cell lines, concentration, time points and assays used (Nerl et al., 2011). The data on the toxicity and genotoxicity of GO are also quite contradictory; there are reports of both low toxicity of GO (Bengtson et al., 2016) and its significant toxicity for different types of cells such as stem cells, germ cells, lung cells, skin cells, endothelial cells and macrophages (Akhavan et al., 2012; Pelin et al., 2017; Ali et al., 2018; Gurunathan et al., 2019).

It is suggested that the toxic effect of NPs can correlate with their ability to penetrate into the cells (Sun et al., 2019). The surface charge of nanomaterials can affect their internalization: positively charged nanomaterials are internalized by cells to a greater extent than are neutral and negatively charged ones (Cho et al., 2009; Sun et al., 2019). Negatively charged membrane proteins directly or indirectly associated with cytoskeleton actin filaments interact with positively charged NPs resulting in NP absorption due to the retrograde motion of microvilli (Orr et al., 2007). According to the zeta-potential data, all the particles used in the present study were negatively charged. However, only clay nanoparticles were readily internalized by cells, while hyperspectral mapping failed to locate carbon nanomaterials inside the cells. The preferential presence of MWCNTs and GO on the cell outside was supported by insignificant changes in cell volume

accompanied by increased cell surface roughness found in AFM and 3D microscopy studies.

Despite the abundance of information on the uptake of nanomaterials by cells, a detailed mechanism of adsorption is not known (Iversen et al., 2011; Sahay et al., 2010). In the study of the transport mechanisms of HNTs in A549 cells it was found that FITC-labeled HNTs were readily internalized into A549 by both clathrin- and caveolae-dependent endocytosis, and the transport pathway of HNTs is an actin- and microtubule-associated process via Golgi apparatus and lysosome (Liu et al., 2019). CNTs can be absorbed through clathrin and/or caveolae-mediated endocytosis/phagocytosis pathway (Verma et al., 2008). The authors of a recent comparative study of MWCNTs and HNTs in cultured endothelial cells and blood vessels concluded that MWCNTs were possibly internalized via clathrin-mediated endocytosis, whereas HNTs were absorbed via energy-dependent non-endocytic uptake (Wu et al., 2020). The less efficient MWCNTs uptake by cells in our study can be explained by both different sizes of the nanotubes (the measured MWCNT hydrodynamic size in the cited study was lower than in our study and averaged around 179.5 nm in water) and cell-specific differences.

The penetration of GO particles can also depend on the cell type. In this work, we observed a low absorption of GO nanoparticles by A549 cells, while GO particles were reported in HCT116 cells and rat skin fibroblasts (Rozhina et al., 2019) as well as in human fibroblast cells (Wang et al., 2010). The absence of GO inside A549 cells was previously mentioned by other researchers (Chang et al., 2011), and the authors suggested that GO interacted with cells on the cell surface or indirectly through other pathways, and partially blocked metabolism in A549 cells. Carbon nanomaterials are prone to agglomeration when prepared without dispersant, which can explain the variability in penetration and toxicity effects observed in different studies (Simon-Deckers et al., 2008), as well as disturbances in the carbon nanotube dose-effect curve (Hirano et

al., 2008). High cytotoxic effect of MWCNTs at low concentrations was observed when penetration of MWCNTs to A549 cells was achieved by dispersing the nanotubes using Arabic gum (Simon-Deckers et al., 2008) or gelatin (Magrez et al., 2006). Oppositely, no acute toxicity on cell viability (WST-1, PI-staining) upon incubation with aggregated MWCNTs was observed, but a dose- and time-dependent increase of intracellular reactive oxygen species (ROS) and decrease of the mitochondrial membrane potential were registered (Pulskamp et al., 2007).

Despite the pronounced internalization of nanoclays by cells, nanoclays demonstrated low cytotoxicity in a colorimetric MTS test which was confirmed by flow cytometry data. Very low toxicity of HNTs was evidenced by many years of research (Vergaro et al., 2012). Platy K particles were previously found to be non-toxic for *Paramecium caudatum* and cancer cell lines and even capable of decreasing the toxicity of GO nanosheets to cells during joint incubation (Kryuchkova et al., 2016; Rozhina et al., 2019). Both clay nanoparticles induced a slight DNA damage, and the tubular nanoclay demonstrated less DNA damaging potency that the platy one. The %tail DNA values found previously in different studies for kaolinite treated cells depended not only on the cell type and the Kaol concentration, but also on the size and morphology of platy Kaol particles (Kato et al., 2017; Kawanishi et al., 2020). Thus, one-hour treatment with Kaol particles increased DNA damage in Chinese hamster ovary CHO AA8 cells and in human primary epidermal keratinocytes and fibroblasts, with Kaol nanoparticles (200 nm) having higher DNA damaging potency and inducing more ROS than Kaol microparticles (4.8 μm) (Kawanishi et al., 2020). Although the low direct genotoxicity of platy Kaol particles towards A549 cells was observed previously (Kato et al., 2017), DNA damaging capacity of Kaol particles to lung cells may be increased *in vivo* (Totsuka et al., 2009; 2011) by Kaol interaction with macrophage cells (Kato et al., 2017).

The introduction of MWCNTs and GO into the incubation medium led to maximum damage to DNA strands in the cells. Moreover, platy GO nanoparticles were found to be the most toxic to A549 cells according to both MTS and flow cytometry data. A high percentage of apoptosis in GO-treated cells was supported by a high degree of DNA damage induced by GO treatment. DNA damage observed in case of CNT treatment did not result in increased apoptosis, indicating that the DNA lesions were probably not irreparable in this case; otherwise they would trigger apoptotic cell death (Norbury and Zhivotovsky, 2004).

The alkaline Comet assay allowed us to assess the general genotoxicity of nanomaterials while further researches are needed to determine the mechanisms of DNA damage in the presence of various nanomaterials. There are two variants of the Comet assay: the neutral and the alkaline one. The alkaline Comet assay is applied to detect DNA single strand breaks, double strand breaks and alkali labile sites, while the neutral assay detects double strand breaks. However, the double-strand break specificity of the neutral Comet assay was put into doubt because the appearance of a DNA segment either in the tail or head of the comet is essentially determined by the relaxation of DNA supercoils and extension of DNA loops, which do not depend on pH (Collins et al., 2008). Instead, such methods as the analysis of foci produced by phosphorylated histone 2A family member X (gamma-H2AX) and tumor suppressor p53 binding protein 1 (53BP1) by immunofluorescence microscopy can be applied to detect double-strand breaks of DNA (Rothkamm et al., 2015).

It is likely that the observed DNA damage was associated with the formation of ROS in the presence of carbon nanomaterials in cell media. It was shown that G and GO nanosheets caused DNA damage by generating ROS both in cells and in zebrafish larvae (Lu et al., 2017). Numerous studies have shown that CNT can induce ROS generation in multiple cell lines and activation of ROS-related intracellular signaling pathways

(Shvedova et al., 2012; Clift et al., 2014). GO induced genotoxicity in normal lung fibroblast cells assessed using the Comet assay at concentration as low as 1µg mL^{-1} (Wang et al., 2013). MWCNTs also induced DNA damage (according to the results of the Comet assay and Micronuclei assay) and cytotoxicity in healthy male human peripheral blood lymphocytes, associated with elevated intracellular ROS level (Kim et al., 2016). MWCNTs were found to be more cytotoxic and genotoxic for immortalized Chinese hamster lung fibroblast V79 cell line and SHE (Syrian hamster embryo) cells than single-walled and double-walled carbon nanotubes, and genotoxicity was seen to increase with CNT width (Darne et al., 2014). In addition, it was reported that CNTs can adsorb nutrients from the medium, resulting in serious toxicity to HepG2 cells (Guo et al., 2008). This effect was not observed for GO, when it was introduced into the A549 cell incubation medium (Chang et al., 2011).

Thus, despite the lower cell penetration of carbon nanomaterials, they had a higher cytotoxic and genotoxic effect than tubular and platy nanoclays. Induction of intracellular oxidative stress is a key event in the toxic effect of nanomaterials (Sharifi et al., 2012). It was demonstrated that GO can cause a dose-dependent oxidative stress in A549 cells even without entering the cells, by inducing generation of reactive oxygen species in culture medium, which then promotes ROS production inside cells (Chang et al., 2011). In turn, oxidative stress caused by particle exposure can trigger a cascade of responses, for example, stimulate an increase in the concentration of cytosolic calcium (Brown et al., 2007) or induce translocation of transcription factors (e.g., NF-κB), regulating anti-inflammatory genes such as TNF-α and iNOS, into the nucleus (Castranova, 2004). Excessive oxidative stress can also alter proteins, lipids, and nucleic acids, which further stimulates the antioxidant defense systems or lead to cell death as a result of apoptosis, necrosis, or inflammatory reactions (Simm and Brömme, 2005; Samuel et al., 2020).

5. Conclusion

529 The purpose of this study was to compare the absorption and cytotoxic effects in lung
530 cancer cells (A549) of four commonly used nanomaterials: carbon nanomaterials
531 (MWCNT and GO) and aluminosilicates (HNT and Kaol). This allows determination of
532 NPs which are the most suitable for use as a carrier system for the delivery of therapeutic
533 agents. All nanomaterials evoked some cytotoxic effects in cells, but the mechanisms of
534 cytotoxicity varied depending on the type of nanomaterial. Despite the lower cell
535 penetration of carbon nanomaterials, they had higher cytotoxic and genotoxic effects,
536 while aluminosilicates were actively absorbed by cells without causing serious damage.
537 Generally, for a certain nanomaterial, the higher its cell penetration, the higher the
538 cytotoxic effect. But when different nanomaterials are compared, the relative toxicity of a
539 nanomaterial is influenced by various factors such as the nanomaterial shape, size and
540 surface chemistry (Sun et al., 2019). As the shapes and sizes of clay and carbon
541 nanoparticles were similar, the higher toxicity of carbon nanomaterials was probably
542 related to their surface chemistry. Although the penetration of carbon nanomaterials was
543 negligible, single CNTs and GO particles were still detected inside cells. We suggest that
544 even this low penetration of carbon nanomaterials was enough to cause some toxic
545 effects, while a much higher penetration of clay nanoparticles was safer to cells. The
546 lower toxicity of the nanoclays allows for considering aluminosilicates of different
547 morphologies as perspective candidates for the delivery of drug compounds or
548 nucleotides. However, *in vitro* assays are only a necessary early step in screening NP
549 cytotoxicity due to their speed, convenience and low cost in comparison with *in vivo* tests
550 (Fard et al., 2015). After finding the safest nanoparticulate candidates for drug delivery in
551 preliminary screenings, more complex studies are required, including co-culture models,
552 3D models and eventually *in vivo* assays, because the interaction with serum proteins
553 and formation of a "protein corona" can dramatically change NP properties. At the same

time, the interaction of NPs with immune cells, patrolling most of the body parts, can cause unexpected effects, not foreseen in *in vitro* studies.

Funding. This study was funded by RFBR (Grant# 18-53-80067 BRICS_t) and the National Natural Science Fund BRICS STI Framework Program of China (No. 51861145304).

Acknowledgement. We thank Prof. Yuri Lvov (Louisiana Technical University) for fruitful discussions and technical help with 3D LSCM. We thank Ms. Farida Akhatova for technical help with AFM.

Declaration of Competing Interest

The authors declare no conflict of interest.

References

Akhatova, F., Danilushkina, A., Kuku, G., Saricam, M., Culha, M., Fakhrullin, R., 2018. Simultaneous intracellular detection of plasmonic and non-plasmonic nanoparticles using dark-field hyperspectral microscopy. Bulletin of the Chemical Society of Japan 91(11), 1640–1645.

Akhavan, O., Ghaderi, E., Akhavan, A., 2012. Size-dependent genotoxicity of graphene nanoplatelets in human stem cells. Biomaterials 33, 8017–8025.

Ali, D., Alarifi, S., Alkahtani, S., Almeer, R.S., 2018. Silver-doped graphene oxide nanocomposite triggers cytotoxicity and apoptosis in human hepatic normal and carcinoma cells. Int. J. Nanomed. 13, 5685–5699.

578 Allen, T.M., Cullis, P.R., 2004. Drug delivery systems: entering the mainstream. Science
579 303 (5665), 1818–1822.

580 Awad, M.E., López-Galindo, A., Setti, M., El-Rahmany, M.M., Iborra, C.V. 2017. Kaolinite
581 in pharmaceutics and biomedicine. Int. J. Pharmaceutics 533, 34-48.

582 Azqueta, A., Dusinska, M. 2015. The use of the comet assay for the evaluation of the
583 genotxicity of nanomaterials. Front. Genet. 6, 239.

584 Balthasar, S., Michaelis, K., Dinauer, N., von Briesen, H., Kreuter, J., Langer, K., 2005.
585 Preparation and characterisation of antibody modified gelatin nanoparticles as drug
586 carrier system for uptake in lymphocytes. Biomaterials 26(15), 2723–2732.

587 Basnet, M., Gershanov, A., Wilkinson, K.J., Ghoshal, S., Tufenkji, N., 2016. Interaction
588 between palladium-doped zerovalent iron nanoparticles and biofilm in granular porous
589 media: characterization, transport and viability. Environ. Sci.: Nano 3, 127–137.

590 Batasheva, S., Kryuchkova, M., Fakhrullin, R., Cavallaro, G., Lazzara, G., Akhatova, F.,
591 Nigamatzyanova, L., Evtugyn, V., Rozhina, E., Fakhrullin, R. 2020. Facile fabrication of
592 natural polyelectrolyte-nanoclay composites: halloysite nanotubes, nucleotides and DNA
593 study. Molecules 25, E3557.

594 Bengtson, S., Kling, K., Madsen, A.M., Noergaard, A.W., Jacobsen, N.R., Clausen, P.A.,
595 Alonso, B., Pesquera, A., Zurutuza, A., Ramos, R., Okuno, H., Dijon, J., Wallin, H., Vogel,
596 U., 2016. No cytotoxicity or genotoxicity of graphene and graphene oxide in murine lung
597 epithelial FE1 cells in vitro. Environ. Mol. Mutagenesis 57(6), 469–482.

598 Berridge, M.V., Tan, A.S. 1993. Characterization of the cellular reduction of 3-(4,5-
599 dimethylthiazol-2-yl)-2,5-diphenyltetrazolium bromide (MTT): subcellular localization,
600 substrate dependence, and involvement of mitochondrial electron transport in MTT
601 reduction. Arch. Biochem. Biophys. 303, 474–82.

602 Berridge, M.V., Herst, P.M., Tan, A.S. 2005. Tetrazolium dyes as tools in cell biology:
603 new insights into their cellular reduction. Biotechnol. Annu. Rev. 11, 127–52.

604 Brown, D.M., Hutchison, L., Donaldson, K., MacKenzie, S.J., Dick, C.A.J., Stone, V.,
605 2007. The effect of oxidative stress on macrophages and lung epithelial cells: The role of
606 phosphodiesterases 1 and 4. Toxicol. Lett. 168 (1), 1–6.

607 Card, J.W., Zeldin, D.C., Bonner, J.C., Nestmann, E.R. 2008. Pulmonary applications and
608 toxicity of engineered nanoparticles. Am. J. Physiol. Lung Cell Mol. Physiol. 295, L400-
609 L411.

610 Casey, A., Herzog, E., Davoren, M., Lyng, F.M., Byrne, H.J., Chambers, G. 2007.
611 Spectroscopic analysis confirms the interaction between single walled carbon nanotubes
612 and various dyes commonly used to assess cytotoxicity. Carbon 45, 1425-1432.

613 Castranova, V., 2004. Signaling pathways controlling the production of inflammatory
614 mediators in response to crystalline silica exposure: role of reactive oxygen/nitrogen
615 species. Free Radic Biol Med. 37(7), 916–925.

616 Cervini-Silva, J., Nieto-Camacho, A., Palacios, E., Montoya, A., Gómez-Vidales, V.,
617 Ramírez-Apán, M.T. 2013. Anti-inflammatory and anti-oxidant activity, and cytoxicity of
618 halloysite surfaces. Colloids Surf B Biointerfaces 111, 651-655.

619 Cervini-Silva, J., Nieto-Camacho, A., Ramírez-Apan, M.T. 2015. The anti-inflammatory
620 properties of different naturally-occurring halloysites. In Research Progress in Natural
621 Mineral Nanotubes. Pasbakhsh P & Churchman J, Editors. Apple Press, New York, Ch.
622 24.

623 Cervini-Silva, J., Nieto-Camacho, A., Palacios, E., del Angel, P., Pentrak, M., Pentrakova,
624 L., Kaufhold, S., Ufer, K., Ramírez-Apan, M.T., Gómez-Vidales, V., Rodríguez Montaño,
625 D., Montoya, A., Stucki, J.W., Theng, B.K.G. 2016. Anti-inflammatory, antibacterial, and

626 cytotoxic activity by natural matrices of nano-iron (hydr)oxide/halloysite. Appl. Clay Sci.
627 120, 101-110.

628 Chang, Y., Yang, S.T., Liu, J.H., Dong, E., Wang, Y., Cao, A., Liu, Y., Wang, H., 2011. In
629 vitro toxicity evaluation of graphene oxide on A549 cells. Toxicol. Lett. 200(3), 201–210.

630 Chen, Y., Qi, Y., Tai, Z., Yan, X., Zhu, F., Xue, Q., 2012. Preparation, mechanical
631 properties and biocompatibility of graphene oxide/ultrahigh molecular weight
632 polyethylene composites. Eur. Polym. J. 48(6), 1026–1033.

633 Cho, E.C., Xie, J.W., Wurm, P.A., Xia, Y.N., 2009. Understanding the role of surface
634 charges in cellular adsorption versus internalization by selectively removing gold
635 nanoparticles on the cell surface with a I2/KI etchant. Nano Lett. 9(3), 1080–1084.

636 Choi, G., Kim, T.-H., Oh, J.-M., Choy, J.-H., 2018. Emerging nanomaterials with advanced
637 drug delivery functions; focused on methotrexate delivery. Coordination Chemistry
638 Reviews 359, 32–51.

639 Clift, M.J.D., Endes, C., Vanhecke, D., Wick, P., Gehr, P., Schins, R.P.F., Petri-Fink, A.,
640 Rothen-Rutishauser, B., 2014. A comparative study of different in vitro lung cell culture
641 systems to assess the most beneficial tool for screening the potential adverse effects of
642 carbon nanotubes. Toxicol. Sci. 137(1), 55–64.

643 Collins, A.R., Oscoz, A.A., Brunborg, G., Gaivao, I., Giovannelli, L., Kruszewski, M.,
644 Smith, C.C., Štětina, R. 2008. The comet assay: topical issues. Mutagenesis 23(3), 143-
645 151.

646 Cornejo-Garrido, H., Nieto-Camacho, A., Gómez-Vidales, V., Ramírez-Apan, M.T., del
647 Angel-Vicente, P., Montoya-de la Fuente, J.A., Domínguez-López, M., Kibanova, D.,
648 Cervini-Silva, J. 2012. The anti-inflammatory properties of halloysite. Appl. Clay Sci. 57,
649 10-16.

650 Darne, C., Terzetti, F., Coulais, C., Fontana, C., Binet, S., Gaté, L., Guichard, Y. 2014.
651 Cytotoxicity and genotoxicity of panel of single- and multiwalled carbon nanotubes: in
652 vitro effects on normal Syrian hamster embryo and immortalized V79 hamster lung cells.
653 J. Toxicol. 2014, 872195.

654 Dhawan, A., Bajpayee, M., Parmar, D., 2009. Comet assay: a reliable tool for the
655 assessment of DNA damage in different models. Cell. Biol. Toxicol. 25, 5–32.

656 Dreyer, D.R., Park, S., Bielawski, C.W., Ruoff, R.S., 2010. The chemistry of graphene
657 oxide. Chem. Soc. Rev. 39(1), 228–240.

658 Fard, J.K., Jafari, S., Eghbal, M.A., 2015. A review of molecular mechanisms involved in
659 toxicity of nanoparticles. Adv. Pharm. Bull. 5(4), 447–454.

660 Gatoo, M.A., Naseem, S., Arfat, M.Y., Dar, A.M., Qasim, K., Zubair, S. 2014.
661 Physicochemical properties of nanomaterials: implication in associated toxic
662 manifestations. BioMed Res. Int. 2014, 498420.

663 Geim, A.K., Novoselov, K.S., 2007. The rise of graphene. Nat. Mater. 6, 183–191.

664 Guo, L., Bussche, A.V.D., Buechner, M., Yan, A., Kane, A.B., Hurt, R.H., 2008.
665 Adsorption of essential micronutrients by carbon nanotubes and the implications for
666 nanotoxicity testing. Small 4, 721–727.

667 Gurunathan, S., Kang, M.-H., Jeyaraj, M., Kim, J.-H., 2019. Differential cytotoxicity of
668 different sizes of graphene oxide nanoparticles in leydig (TM3) and sertoli (TM4) cells.
669 Nanomaterials 9(2), 139.

670 Hirano, S, Kanno, S, Furuyama, A. 2008. Multi-walled carbon nanotubes injure the
671 plasma membrane of macrophages. Toxicol. Appl. Pharmacol. 232(2), 244–251.

672 Iversen, T.-G., Skotland, T., Sandvig, K., 2011. Endocytosis and intracellular transport of
673 nanoparticles: Present knowledge and need for future studies. Nano Today 6 (2), 176–
674 185.

675 Jeevanandam, J., Barhoum, A., Chan, Y.S., Dufresne, A., Danquah, K. 2018. Review on
676 nanoparticles and nanostructured materials: history, sources, toxicity and regulations.
677 Beilstein J. Nanotechnol. 9, 1050-1074.

678 Kato, T., Toyooka, T., Ibuki, Y., Masuda, S., Watanabe, M., Totsuka, Y. 2017. Effect of
679 physicochemical caracter differences on the genotocix potency of kaolinite. Genes and
680 Environment 39, 12.

681 Kawanishi, M., Yoneda, R., Totsuka, Y., Yagi, T. 2020. Genotoxicity of micro- and nano-
682 particles of kaolinite in human primary dermal keratinocytes and fibroblasts. Genes and
683 Environ. 42, 16.

684 Kayat, J., Gajbhiye, V., Tekade, R.K., Jain, N.K., 2011. Pulmonary toxicity of carbon
685 nanotubes: a systematic report. Nanomedicine: NBM, 7(1), 40–49.

686 Khodzhaeva, V., Makeeva, A., Ulyanova, V., Zelenikhin, P., Evtugyn, V., Hardt, M.,
687 Rozhina, E., Lvov, Y., Fakhrullin, R., Ilinskaya, O., 2017. Binase immobilized on halloysite
688 nanotubes exerts enhanced cytotoxicity toward human colon adenocarcinoma cells.
689 Front. Pharmacol. 8, 631.

690 Kim, J.S., Song, K.S., Yu, I.J. 2016. Multiwall carbon nanotube-induced DNA damage
691 and cytotoxicity in male human peripheral blood lymphocytes. Int. J. Toxicol. 35, 27-37.

692 Kryuchkova, M., Danilushkina, A., Lvov, Y., Fakhrullin, R. 2016. Evaluation of toxicity of
693 nanoclays and graphene oxide in vivo: a Paramecium caudatum study. Environ. Sci.:
694 Nano. 3, 442-452.

695 Kryuchkova, M., Fakhrullin, R., 2018. Kaolinite alleviates graphene oxide toxicity.
696 Environ. Sci. Technol. Lett. 5, 295–300.

697 Kryuchkova, M.; Batasheva, S.; Naumenko, E.; Rozhina, E.; Akhatova, F.; Panchal, A.;
698 Lvov, Y.; Fakhrullin, R. 2020. Self-assembly of concentric microrings of tubule and platy
699 nanoclays for cell patterning and capturing. Appl. Clay Sci. 195, 105707.

700 LaVan, D., McGuire, T., Langer, R., 2003. Small-scale systems for in vivo drug delivery.
701 Nat Biotechnol. 21, 1184–1191.

702 Li, J., Cai, C., Li, J., Li, J., Li, J., Sun, T., Wang, L., Wu, H., Yu, G., 2018. Chitosan-based
703 nanomaterials for drug delivery. Molecules 23(10), 2661.

704 Liu, H., Wang, Z.-G., Liu, S.-L., Yao, X., Chen, Y., Shen, S., Wu, Y., Tian, W. 2019.
705 Intracellular pathway of halloysite nanotubes: potential application for antitumor drug
706 delivery. J. Mater. Sci. 54, 693-704.

707 Liu, Z., Robinson, J.T., Sun, X., Dai, H., 2008. PEGylated nanographene oxide for
708 delivery of water-insoluble cancer drugs. J. Am. Chem. Soc. 130(33), 10876–10877.

709 Lu, C.J., Jiang, X.F., Junaid, M., Ma, Y.B., Jia, P.P., Wang, H.B., Pei D.S., 2017.
710 Graphene oxide nanosheets induce DNA damage and activate the base excision repair
711 (BER) signaling pathway both in vitro and in vivo. Chemosphere 184, 795–805.

712 Lvov, Y.M., DeVilliers, M.M.,Fakhrullin, R.F. 2016. The application of halloysite tubule
713 nanoclay in drug delivery. Expert Opin. Drug Deliv. 13, 977-986.

714 Magrez, A., Kasas, S., Salicio, V., Pasquier, N., Seo, J.W., Celio, M., Catsicas, S.,
715 Schwaller, B., Forro, L., 2006. Cellular toxicity of carbon-based nanomaterials. Nano Lett.
716 6, 1121–1125.

717 Maisanaba, S., Pichardo, S., Puerto, M., Gutierrez-Praena, D., Camean, A.M., Jos, A.
718 2015. Toxicological evaluation of clay minerals and derived nanocomposites: a review.
719 Environ. Res. 138, 233-254.

720 Massaro, M.; Barone, G.; Biddeci, G.; Cavallaro, G.; Di Blasi, F.; Lazzara, G.; Nicotra, G.;
721 Spinella, C.; Spinelli, G.; Riela, S. 2019. Halloysite nanotubes-carbon dots hybrids
722 multifunctional nanocarrier with positive cell target ability as a potential non-viral vector
723 for oral gene therapy. J. Colloid. Interface Sci. 552, 236–246.

724 Meindl, C., Absenger, M., Roblegg, E., Fröhlich, E. 2013. Suitability of cell-based label-
725 free detection for cytotoxicity screening of carbon nanotubes. BioMed Res. Int. 2013,
726 564804.

727 Mohajeri, M., Behnam, B., Sahebkar, A., 2018. Biomedical applications of carbon
728 nanomaterials: Drug and gene delivery potentials. J. Cell. Physiol. 234 (1), 298–319.

729 Murray, H., 2000. Traditional and new applications for kaolinite, smectite, and
730 palygorskite: A general overview. Appl. Clay Sci. 17(5), 207–221.

731 Nandhakumar, S., Parasuraman, S., Shanmugam, M.M., Ramachandra Rao, K., Chand,
732 P., Vishnu Bhat, B. 2011. Evaluation of DNA damage using single-cell gel electrophoresis
733 (Comet Assay). j. Pharmacol. Pharmacother. 2, 107-111.

734 Naumenko, E.; Fakhrullin, R. 2019. Halloysite nanoclay/biopolymer composite materials
735 in tissue engineering. Biotechnol. J. 14, 1900055.

736 Nerl, H.C., Cheng, C., Goode, A.E., Bergin, S.D., Lich, B., Gass, M., Porter, A.E. 2011.
737 Imaging methods for determining uptake and toxicity of carbon nanotubes in vitro and in
738 vivo. Nanomedicine 6, 849-865.

739 Norbury, C.J., Zhivotovsky, B. 2004. DNA damage-induced apoptosis. Oncogene 23,
740 2797-2808.

741 Oh, W.K., Kim, S., Yoon, H., Jang, J., 2010. Shape-dependent cytotoxicity and
742 proinflammatory response of poly(3,4-ethylenedioxythiophene) nanomaterials. Small 6,
743 872–879.

744 Orr, G., Panther, D.J., Phillips, J.L., Tarasevich, B.J., Dohnalkova, A., Hu, D.,
745 Teeguarden, J.G., Pounds, J.G., 2007. Submicrometer and nanoscale inorganic particles
746 exploit the actin machinery to be propelled along microvilli-like structures into alveolar
747 cells. ACS Nano 1 (5), 463–475.

748 Pacurari, M., Yin, X.J., Ding, M., Leonard, S.S., Schwegler-Berry, D., Ducatman, B.S.,
749 Chirila, M., Endo, M., Castranova, V., Vallyathan, V. 2008. Oxidative and molecular
750 interactions of multi-wall carbon nanotubes (MWCNT) in normal and malignant human
751 mesothelial cells. Nanotoxicology 2, 155-170.

752 Panchal, A.; Fakhrullina, G.; Fakhrullin, R.; Lvov, Y. 2018. Self-assembly of clay
753 nanotubes on hair surface for medical and cosmetic formulations. Nanoscale 10, 18205–
754 18216.

755 Park, S., Ruoff, R.S., 2009. Chemical methods for the production of graphenes. Nat.
756 Nanotechnol. 4(4), 217–224.

757 Pelin, M., Fusco, L., León, V., Martín, C., Criado, A., Sosa, S., Vázquez, E., Tubaro, A.,
758 Prato, M., 2017. Differential cytotoxic effects of graphene and graphene oxide on skin
759 keratinocytes. Sci. Rep. 7, 40572.

760 Pulskamp, K., Diabate, S., Krug, H.F., 2007. Carbon nanotubes show no sign of acute
761 toxicity but induce intracellular reactive oxygen species in dependence on contaminants.
762 Toxicol. Lett. 168, 58–74.

763 Rahikkala, A., Rosenholm, J.M., Santos, H.A., 2018. Biofunctionalized mesoporous silica
764 nanomaterials for targeted drug delivery. In: Sarmento, B., das Neves, J. (Ed.),
765 Biomedical Applications of Functionalized Nanomaterials, pp. 489–520 (Chapter 16).

766 Richard, J. P., Melikov, K., Vives, E., Ramos, C., Verbeure, B., Gait, M.J., Chernomordik,
767 L.V., Lebleu, B. 2003. Cell-penetrating Peptides. A reevaluation of the mechanism of
768 cellular uptake. J. Biol. Chem. 278(1), 585–590.

769 Rothkamm, K., Barnard, S., Moquet, J., Ellender, M., Rana, Z., Burdak-Rothkamm, S.
770 2015. DNA damage foci: Meaning and significance. Environ. Mol. Mutagen 56(6), 491-
771 504.

772 Rozhina, E., Batasheva, S., Danilushkina, A., Kryuchkova, M., Gomzikova, M.,
773 Cherednichenko, Y., Nigamatzyanova, L., Akhatova F., Fakhrullin, R., 2019. Kaolinite
774 alleviates the toxicity of graphene oxide for mammalian cells. Med. Chem. Comm.10,
775 1457–1464.

776 Rozhina, E.; Panchal, A.; Akhatova, F.; Lvov, Y.; Fakhrullin, R. 2020. Cytocompatibility
777 and cellular uptake of alkylsilane-modified hydrophobic halloysite nanotubes. Appl. Clay
778 Sci. 185, 105371.

779 Sahay, G., Alakhova, D.Y., Kabanov, A.V., 2010. Endocytosis of nanomedicines. J.
780 Controlled Release 145 (3), 182–195.

781 Samuel, M.S., Selvarajan, E., Subramaniam, K., Mathimani, T., Seethappan, S.,
782 Pugazhendhi, A., 2020. Synthesized β-cyclodextrin modified graphene oxide (β-CD-GO)
783 composite for adsorption of cadmium and their toxicity profile in cervical cancer (HeLa)
784 cell lines. Process Biochemistry 93, 28–35.

785 Sharifi, S., Behzadi, S., Laurent, S., Forrest, M.L., Stroeve, P., Mahmoudi, M. 2012.
786 Toxicity of nanomaterials. Chem. Soc. Rev. 41, 2323-2343.

787 Shvedova, A.A., Pietroiusti, A., Fadeel, B., Kagan, V.E., 2012. Mechanisms of carbon
788 nanotube-induced toxicity: focus on oxidative stress. Toxicol. Appl. Pharmacol. 261(2),
789 121-133.

790 Simm, A., Brömme, H.J., 2005. Reactive oxygen species (ROS) and aging: Do we need
791 them — can we measure them — should we block them? Signal Transduction 5 (3), 115–
792 125.

793 Simon-Deckers, A., Gouget, B., Mayne-L'Hermite, M., Herlin-Boime, N., Reynaud, C.,
794 Carrière, M. 2008. In vitro investigation of oxide nanoparticle and carbon nanotube toxicity
795 and intracellular accumulation in A549 human pneumocytes. Toxicology 253, 137-146.

796 Smith, R., Ghosn, E.E.B., Rallapalli, H., Prescher, J.A., Larson, T., Herzenberg, L.A.,
797 Gambhir, S.S., 2014. Selective uptake of single walled carbon nanotubes by circulating
798 monocytes for enhanced tumour delivery. Nat. Nanotechnol. 9 (6), 481–487.

799 Stankovich, S., Dikin, D.A., Dommett, G.H., Kohlhaas, K.M., Zimney, E.J., Stach, E.A.,
800 Piner, R.D., Nguyen, S.T., Ruoff, R.S., 2006. Graphene-based composite materials.
801 Nature 442(7100), 282–286.

802 Su, C.L., Loh, K.P., 2013. Carbocatalysts: graphene oxide and its derivatives. Acc. Chem.
803 Res. 46(10), 2275–2285.

804 Sun, H., Jiang, C., Wu, L., Bai, X., Zhai, S. 2019. Cytotoxicity-related bioeffects induced
805 by nanoparticles: The role of surface chemistry. Front. Bioeng. Biotechnol. 7, 414.

806 Tarasova, E., Naumenko, E., Rozhina, E., Akhatova, F., Fakhrullin, R., 2019.
807 Cytocompatibility and uptake of polycations-modified halloysite clay nanotubes. Appl.
808 Clay Sci. 169, 21–30.

809 Thambi, T., Park, J.H., 2014. Recent advances in shell-sheddable nanoparticles for
810 cancer therapy. J. Biomed. Nanotechnol. 10 (9), 1841–1862.

811 Totsuka, Y., Higuchi, T., Imai, T., Nishikawa, A., Nohmi, T., Kato, T., Masuda, S., Kinae,
812 N., Hiyoshi, K., Ogo, S., Kawanishi, M., Yagi, T., Ichinose, T., Fukumori, N., Watanabe,
813 M., Sugimura, T., Wakabayashi, K. 2009. Genotoxicity of nano/microparticles in in vitro
814 micronuclei, in vivo comet and mutation assay systems. Particle and Fibre Toxicology 6,
815 23.

816 Totsuka, Y., Kato, T., Masuda, S., Ishino, K., Matsumoto, Y., Goto, S., Kawanishi, M.,
817 Yagi, T., Wakabayashi, K. 2011. In vitro and in vivo genotoxicity induced by fullerene
818 (C60) and kaolinite // Genes and Environ. 33, 14-20.

819 Vergaro, V., Lvov, Y., Leporatti, S., 2012. Halloysite clay nanotubes for resveratrol
820 delivery to cancer cells. Macromol. Biosci. 12, 1265–1271.

821 Verma, A., Uzun, O., Hu, Y., Hu, Y., Han, H.-S., Watson, N., Chen, S., Irvine, D.J.,
822 Stellacci, F., 2008. Surface-structure-regulated cell-membrane penetration by monolayer-
823 protected nanoparticles. Nat. Mater. 7(7), 588–595.

824 Wang, A., Pu, K., Dong, B., Liu, Y., Zhang, L., Zhang, Z., Duan, W., Zhu, Y. 2013. Role
825 of surface charge and oxidative stress in cytotoxicity and genotoxicity of graphene oxide
826 towards human lung fibroblast cells. J. Appl. Toxicol. 33, 1156-1164.

827 Wang, K., Ruan, J., Song, H., Zhang, J., Wo, Y., Guo, S., Cui, D., 2010. Biocompatibility
828 of graphene oxide. Nanoscale Res. Lett. 6(1), 8.

829 Wang, Z., Luo, T., Cao, A., Sun, J., Jia, L., Sheng, R., 2018. Morphology-variable
830 aggregates prepared from cholesterol-containing amphiphilic glycopolymers: Their
831 protein recognition/adsorption and drug delivery applications. Nanomaterials 8(3), 136.

832 Wörle-Knirsch, J.M., Pulskamp, K., Krug, H.F. 2006. Oops they did it again! Carbon
833 nanotubes hoax scientists in viability assays. Nano Letters 6, 1261-1268.

834 Wu, B., Jiang, M., Liu, X., Huang, C., Gu, Z., Cao, Y. 2020. Evaluation of toxicity of
835 halloysite nanotubes and multi-walled carbon nanotubes to endothelial cells in vitro and
836 blood vessels in vivo // Nanotoxicology, DOI: 10.1080/17435390.2020.1780642.

837 Xia, T., Kovochich, M., Brant, J., Hotze, M., Sempf, J., Oberley, T., Sioutas,C., Yeh, J.I.,
838 Wiesner, M.R., Nel, A.E., 2006. Comparison of the abilities of ambient and manufactured
839 nanoparticles to induce cellular toxicity according to an oxidative stress paradigm. Nano
840 Lett. 6 (8), 1794–1807.

841 Xu, S., Yu, X., Chen, Z., Zeng, Y., Guo, L., Li, L., Luo, F., Wang, J., Qiu, B., Lin, Z., 2020.
842 Real-time visualization of the single-nanoparticle electrocatalytic hydrogen generation
843 process and activity under dark field microscopy. Analytical Chemistry.
844 doi:10.1021/acs.analchem.0c01129.

845 Yang, K., Li, Y., Tan, X., Peng, R., Liu, Z., 2013. Behavior and toxicity of graphene and
846 its functionalized derivatives in biological systems. Small 9 (9-10), 1492–1503.

847 Yang, S.T., Luo, J., Zhou, Q., Wang, H., 2012. Pharmacokinetics, metabolism and toxicity
848 of carbon nanotubes for biomedical purposes. Theranostics 2 (3), 271–282.

849 Zhou, C., Choi, Y.S., David, A.E., Todd, P.W., Hanley, T.R. 2018. Nanomaterial
850 endocytosis: Estimation of perticles per cell by magnetic measurement. IEEE Magnetic
851 Letters 9, 1503405.